ACS OMEGA

http://pubs.acs.org/journal/acsodf

Article

Synthesis of a Cd-MOF Fluorescence Sensor and Its Detection of Fe^{3+}, Fluazinam, TNP, and Sulfasalazine Enteric-Coated Tablets in Aqueous Solution

Wen Liu, Hua-li Cui,* Jie Zhou, Zi-tong Su, You-zhen Zhang, Xiao-li Chen, and Er-lin Yue

Cite This: *ACS Omega* 2023, 8, 24635−24643

Read Online

ACCESS | Metrics & More | Article Recommendations | Supporting Information

ABSTRACT: A Cd-based metal−organic framework (Cd-MOF), named after $\{[Cd(ttc)(H_2O)]\cdot H_2O\}_n$ (ttc = 1-imidazole-1-yl-2,4,6-benzene-tricarboxylic acid), was synthesized using the solvothermal reaction. The single-crystal structure was determined by single X-ray diffraction analysis, and crystalline characteristics and composition were confirmed by powder X-ray diffraction (PXRD) and thermogravimetric analysis (TG), respectively. Structural analysis showed that the Cd^{2+} ion is in the seven-coordinated mode, in which ttc^{2-} ion adopts the μ_4-η^1-η^1-η^2-η^2 coordination mode. It is worth noting that the Cd^{2+} ion is connected to ttc^{2-} to form a 2D network, and the adjacent 2D network is expanded into a 3D supramolecular network structure through weak hydrogen bonds. The fluorescence sensing experiments indicated that Cd-MOF could not only be used as a fluorescence sensor for Fe^{3+}, fluazinam (FLU), and 2,4,6-trinitrophenolol (TNP) but also for sulfasalazine detection in aqueous solution. To verify the sensitivity of the fluorescent probe, we calculated its detection limit: 5.34×10^{-8} M (Fe^{3+}), 7.8×10^{-8} M (FLU), 1.21×10^{-7} M (TNP), and 2.67×10^{-7} M (SECT). In addition, the quenching mechanism was thoroughly studied.

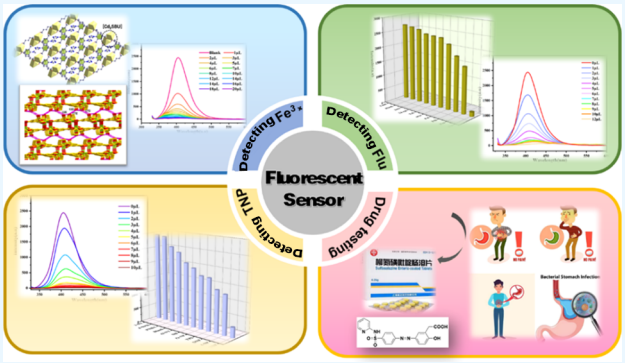

1. INTRODUCTION

With rapid advancements in science and technology and the growth of large enterprises, the number of sources of pollution threatening human health and the environment has steadily increased. Pollutants primarily include heavy metal ions, toxic gases, pesticides, and explosives and highly toxic nitroaromatic compounds.[1]

Iron ions play a critical role in human health and the ecological stability of the environment, and they are necessary for certain enzyme reactions and physiological processes. Iron is also a core component of hemoglobin and is involved in the synthesis of myoglobin, cytochrome, and enzymes. It plays an invaluable role in oxygen transport and participates in metabolic activities in the body. However, excessive amounts of iron ions cannot be metabolized in the body and affect the absorption of other trace elements in the body.[2] Meanwhile, nitroaromatic compounds (NACs) are the most widely used explosives, exhibiting excellent destructive, toxic, and carcinogenic properties. Consequently, they have emerged as a serious source of groundwater and soil pollution.[3−5]

Over the past few decades, anti-inflammatory drugs and pesticides have been widely utilized, with the former to combat human and animal diseases and the latter to prevent foreign invasion in agriculture.[6] However, the overuse and misuse of these chemicals have resulted in high levels of residues in animals and plants, resulting in irreparable damage to the body and environment.[7] For example, FLU may cause irreversible damage to the human body if accidently ingested or exposed to the skin and eyes.[8] Moreover, it is an environmental pollutant. The common symptoms of ulcerative colitis are diarrhea with mucus, pus, bloody stool, and abdominal pain, among several others. Although sulfasalazine enteric-coated tablets (SECTs) are effective drugs for treating ulcerative colitis,[9] excessive use of SECTs can cause severe side effects, such as abnormal red blood cells, dizziness, and tinnitus.[10]

Luminescent metal−organic frameworks (LMOFs) are hybrid materials with porous structures assembled by organic connectors and metal cations through coordination bonds. LMOFs have been widely implemented in various fields such as gas absorption and separation,[11−13] fluorescence detection, biological imaging, and photocatalytic degradation of organic pollutants.[14] Sheldrick et al. reported Eu-MOFs that can selectively sense Fe^{3+} through fluorescence quenching.[15] Alhaddad et al. described a two-dimensional Cd-MOF for selective identification of 4-NP in aqueous environments.[16]

Received: May 4, 2023
Accepted: June 16, 2023
Published: June 28, 2023

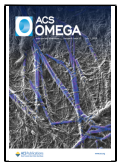

https://doi.org/10.1021/acsomega.3c03073
ACS Omega 2023, 8, 24635−24643

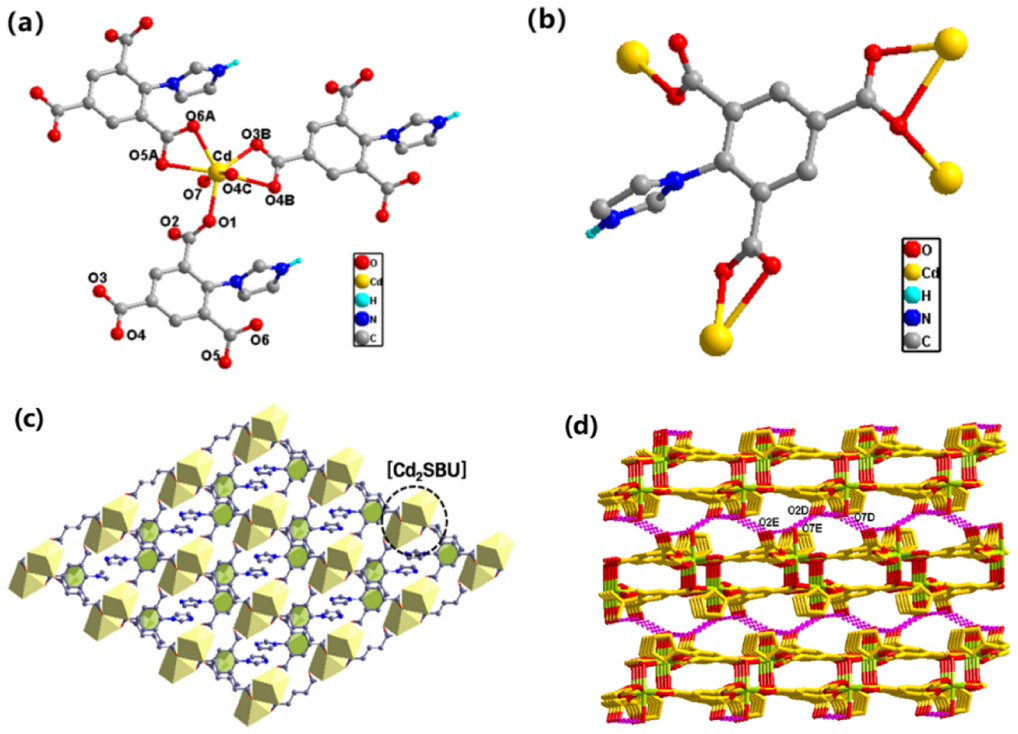

Figure 1. (a) Coordination environment around the Cd^{2+}in Cd-MOF. [Symmetry codes: A (1 + X, Y, Z); B (X, Y, −1 + Z); C (1 − X, 1 − Y, 1 − Z)]; (b) coordination forms of ttc in Cd-MOF; (c) 2D framework of Cd-MOF; (d) 3D supramolecular structures linked by hydrogen bonds [symmetry codes: D (1 + X, 0.5 − Y, 1.5 + Z); E (1 + X, −1 − Y, 1 + Z)].

Present detection devices, such as metal detectors, and techniques, such as gas chromatography, prove costly and inconvenient. Thus, to develop a method for simultaneous and rapid detection of multiple targets in aqueous environments, we synthesized a Cd-MOF that can quickly respond to Fe^{3+}, fluridone (FLU), 2,4,6-trinitrophenol (TNP), and sulfasalazine in water.[17] LMOFs have been previously used to detect cations, nitro explosives, pesticides, and small organic molecules. Therefore, they are the first choice for fluorescence detection.[18]

In the present study, a novel 3D microporous Cd-MOF $\{[Cd(ttc)(H_2O)]\cdot H_2O\}_n$ has been constructed based on the nitrogen-containing tricarboxylic acid ligand, 1-imidazole-1-yl-2,4,6-benzene-tricarboxylic acid, under solvothermal conditions. The crystal structure and luminescence properties of the prepared Cd-MOF were investigated. The prepared Cd-MOF exhibited high sensitivity and selectivity to Fe^{3+}, FLU, TNP, and sulfasalazine through luminescence quenching. In addition, we elucidated the mechanism of the fluorescence quenching of Cd-MOF.

2. EXPERIMENTAL SECTION

2.1. Materials and Instrumentation. The chemicals used in this text are all commercially available and can be used without further purification. PXRD was carried out on a Bruker D8 ADVANCE X-ray diffractometer. Fluorescence experiments were carried out on the Hitachi F-7100 Fluorescence Spectrophotometer. Thermogravimetric analysis (TGA) was performed on a NETZSCH STA 449F5 thermal analyzer. Infrared spectra were obtained on a Shimadzu Affinity-1S spectrophotometer with KBr pellets in the range of 500−4000 cm^{-1}. The UV−vis absorption spectra were measured on a Shimadzu UV-2700 spectrophotometer.

2.2. Synthesis of $\{[Cd(ttc)(H_2O)]\cdot H_2O\}_n$. A solid mixture of Cd $(NO_3)_2$ (0.1 mmol) and ttc (0.05 mmol) was dissolved in a mixed solvent of DMF (4 mL), H_2O (3 mL), and HNO_3 (100 μL). The mixed solution was placed in a 15 mL inner glass bottle and reacted at 95 °C for three days. Finally, colorless crystals are obtained with a yield of 53%. Elemental analysis Calcd for $C_{12}H_{10}N_2O_8Cd$ (%): C, 34.15; H, 2.13; N, 6.64. Found (%): C, 34.13; H, 2.11; N, 6.61. IR (KBr, cm^{-1}): 1930 (w), 1802 (w), 1679 (w), 1608 (s), 1582 (m), 1515 (s), 1400 (s), 1299 (m), 1154 (m), 1105 (m), 1012 (m), 983 (w).

2.3. Crystal Structure Determination. Single crystal data of Cd-MOF were collected on a Bruker SMART APEX-II diffractometer (Mo Kα radiation and λ = 0.71073 Å). The crystal structures were solved using direct methods and then refined by full-matrix least-squares techniques on F^2 using SHELXL. All non-hydrogen atoms were refined anisotropically. Hydrogen atoms were obtained by geometric calculation. All calculations are performed using the SHELXTL program. Table S1 contains crystal data for Cd-MOF. Table S2 contains selected bond lengths and angles. Data deposition number CCDC no: 2213445.

2.4. Fluorescence Sensing Experiments. A mixed solution of 3 mg of ground sample and 10 mL of water was formed and sonicated for 30 min. Then, the solution was left to stand for three days. Finally, the supernatant was used for the fluorescence sensing experiment. In order to ensure the stability of the Cd-MOF material after soaking, we filtered and dried the sample soaked in water for 3 days and performed PXRD characterization (Figure S1). The experiment proves that the structure of the material remains intact after soaking, indicating that the material has good stability in aqueous solutions.

https://doi.org/10.1021/acsomega.3c03073
ACS Omega 2023, 8, 24635−24643

3. RESULTS AND DISCUSSION

3.1. Structural Analysis. According to the results of X-ray single crystal diffraction analysis, the prepared Cd-MOF is a monoclinic crystal of the $P2_1/c$ space group. The asymmetric structure unit consists of one Cd^{2+} ion, one ttc^{2-} ligands, one coordination water molecule, and one free water molecule. In complex Cd-MOF, ttc^{2-} ligands are completely deprotonated and coordinated in the μ_4-η^1-η^1-η^2-η^2 mode, whereas the N atom in the pyridine ring is protonated (Figure 1b). Each Cd^{2+} ion is seven-coordinated in the twisted pentagonal bipyramidal geometry with six oxygen atoms (O6A, O5A, O3B, O4B, O4C, and O1) from four ttc^{2-} ligands and one oxygen atom (O7) from a coordinated water molecule (Figure 1a). Cd−O distances are in the range of 2.2380(15)−2.6106(16) Å, and the corresponding angles (O−Cd−O) changed from 53.13(5) to 173.60(5)°, which are dependent on oxygen atoms located on differently symmetric units from the ttc ligand. Cd^{2+} ions are connected horizontally to carboxylic acid ligands, forming a 2D network (Figure 1c). The hydrogen bonds between layers further expand the 2D network into a 3D supramolecular network (Figure 1d).

3.2. PXRD and TGA of Cd-MOF. The simulated PXRD spectra of Cd-MOF were in good agreement with the experimental spectra (Figure S1), which proves the high purity and crystallinity of the product. The PXRD patterns of the complex after the addition of Fe^{3+}, FLU, and TNP are also shown. The experimental peak coincided well with the initial simulated peak of the complex, indicating that the skeleton of the complex after the fluorescence experiment is complete and exhibits good stability.

The thermal stability of Cd-MOF was studied through TGA (Figure S2). The first weight loss peak (3.64%; Calcd 4.29%) was observed at 179 °C, possibly due to the loss of water molecules. At 305 °C, the skeleton began to decompose and collapse, and the remaining 32% may be CdO (Calcd 32.42%).

3.3. Photoluminescence Properties of Cd-MOF. MOFs with d^{10} metal ions possess excellent luminescence properties. Therefore, we obtained the solid-state fluorescence excitation−emission spectra of the ligands ttc and Cd-MOF at room temperature (Figure 2). The maximum emission peak of ttc is observed at 445 nm (λ_{ex} = 378 nm), whereas Cd-MOF exhibits an emission peak at 423 nm (λ_{ex} = 328 nm), with a slight blue shift ($\Delta\lambda$ = 22 nm) attributed to the metal perturbation emission of the ligand. The emission peak of Cd-MOF is stronger than that of the ligand due to coordination interactions. This was attributed to the meta-ligand charge transfer or ligand−metal charge transfer.[19−23] Owing to the excellent fluorescence characteristics of solid-state Cd-MOF, we have studied its fluorescence sensing performance under an excitation of 328 nm.

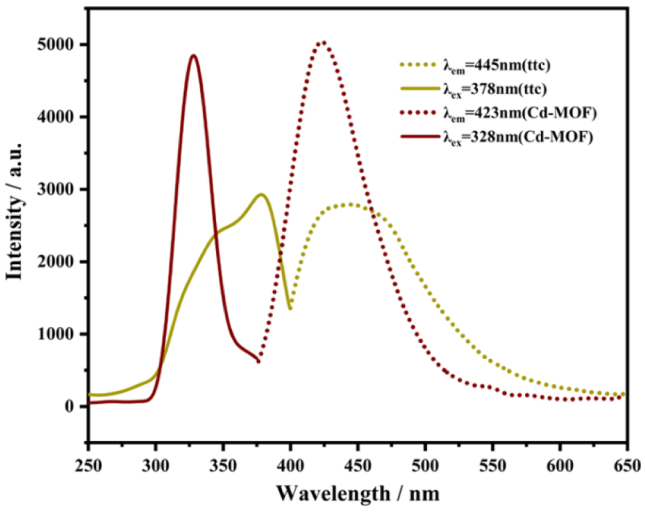

Figure 2. Solid-state fluorescence excitation emission spectra of ligands ttc and Cd-MOF at room temperature.

3.3.1. Fluorescence Detection of Cd-MOF for Different Cations. We prepared solutions (5 mmol/L) of the following 13 cations: Ag^+, Ba^{2+}, Ca^{2+}, Cd^{2+}, Co^{2+}, Fe^{3+}, K^+, La^{3+}, Mg^{2+}, Ni^{2+}, Pb^{2+}, Bi^{3+}, and Zn^{2+} for fluorescence sensing testing. First, 3 mg of ground Cd-MOF was dispersed in 10 mL of distilled water, sonicated for 30 min, and left to stand at room temperature for 3 days before taking the supernatant for fluorescence experiments. Second, qualitative experiments were conducted on Cd-MOF,which was dispersed in a cationic solution. The fluorescence of Cd-MOF was considerably quenched after the addition of Fe^{3+} (Figure 3a). The fluorescence intensity does not show a remarkable variation with the addition of other cations. Therefore, Fe^{3+} caused the most extensive quenching effect, demonstrating that Cd-MOF can be used as a sensor for detecting Fe^{3+} in water. To investigate the effect of Fe^{3+} concentration on the fluorescence intensity of Cd-MOF, a quantitative experiment was conducted. The fluorescence intensity of Cd-MOF gradually decreased as the concentration of Fe^{3+} increased from 0 to 20 μL (Figure 3b). At the Fe^{3+} concentration of 20 μL, the fluorescence intensity of the complex reached the minimum, exhibiting linearity at low concentrations (5×10^{-6} to 3×10^{-5} M) (Figure S3). To further evaluate the effect of luminescent titration, the Stern−Volmer (S−V) equation ($I_0/I = 1 + K_{SV}[M]$) was employed to calculate the quenching efficiency, where I_0 is the initial luminescence intensity,[24−27] I is the luminescence intensity after the addition of Fe^{3+}, $[M]$ is the concentration of Fe^{3+}, and K_{SV} is the quenching constant at the concentration of 100 μM. The calculated K_{SV} and LOD values are 3.327×10^{-5} M and 0.053 μmol/L. Finally, an interference experiment was conducted (Figure S4). We found that the fluorescence intensity did not remarkably decrease with the addition of other cations. However, the addition of equimolar Fe^{3+} resulted in almost complete quenching, indicating that the quenching by Fe^{3+} is not affected by competition with other cations. These results demonstrate that Cd-MOF is a promising fluorescent sensor for Fe^{3+} with high sensitivity and selectivity.

3.3.2. Fluorescence Detection of Cd-MOF for Different Pesticides. The following nine pesticide solutions (10 mmol/L) were prepared for fluorescence sensing tests: pyrazolsteride (Pst), pyrimethanil (Pth), apromazole (Ima), amamectin benzoate (EmB), neutromycin (myc), 2,4-epibrassinolide (2,4-EPI), trizodone (Pro), imidylamine (Tdi), and FLU. First, 3 mg of ground Cd-MOF was dispersed in 10 mL of distilled water, sonicated for 30 min, and left to stand at room temperature for 3 days before taking the supernatant for fluorescence experiments. Second, qualitative experiments were conducted on Cd-MOF, which was dispersed in the prepared pesticide aqueous solutions. The fluorescence of Cd-MOF was remarkably quenched after the addition of FLU (Figure 4a). The fluorescence intensity after the addition of other pesticides does not vary substantially. Therefore, FLU caused the most considerable quenching effect, demonstrating

https://doi.org/10.1021/acsomega.3c03073
ACS Omega 2023, 8, 24635−24643

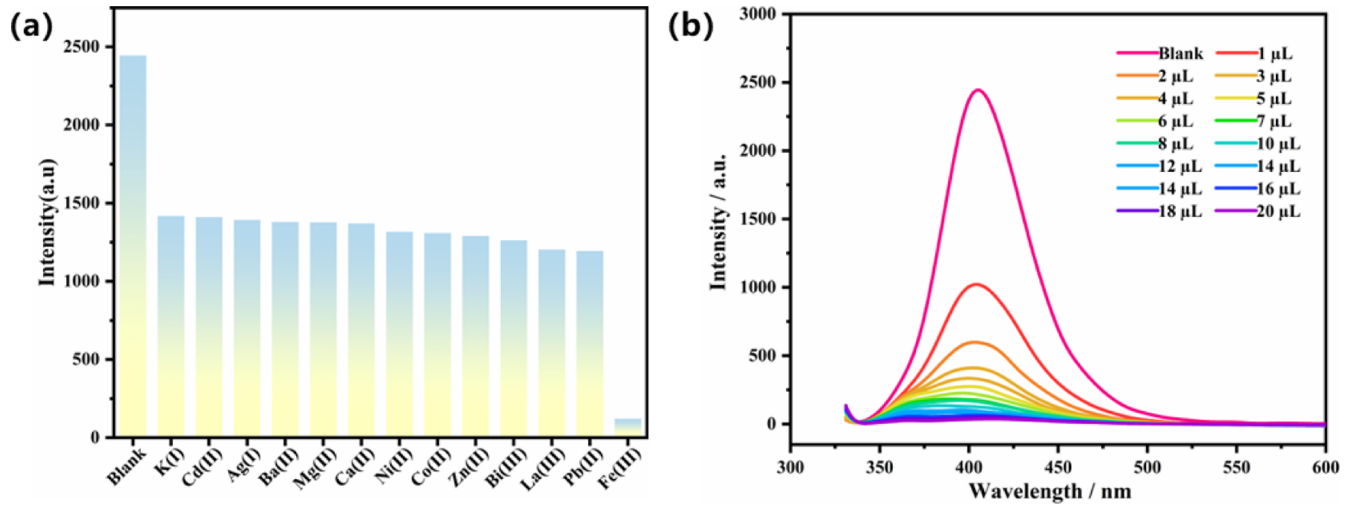

Figure 3. (a) Fluorescence intensity changes of Cd-MOF dispersed in different cationic solutions; (b) change of the luminescence spectrum of Cd-MOF with the concentration of Fe^{3+} solutions.

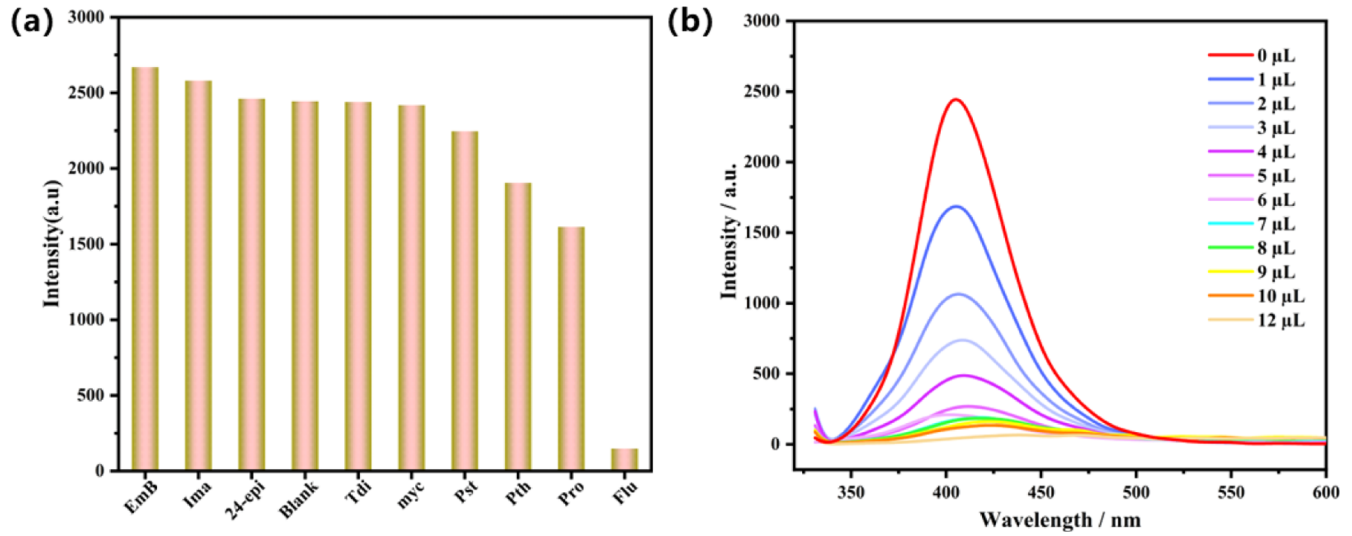

Figure 4. (a) Fluorescence intensity changes of Cd-MOF dispersed in different pesticides solutions; (b) luminescent emission spectra of Cd-MOF dispersed in an aqueous solution upon incremental addition of FLU.

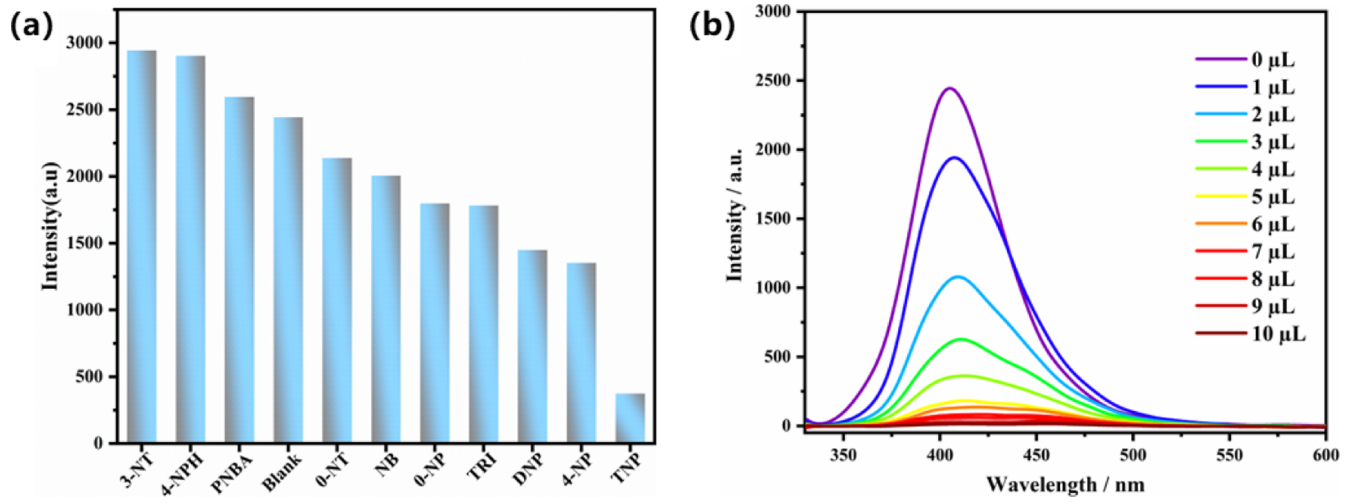

Figure 5. (a) Fluorescence intensity changes of Cd-MOF dispersed in different NACs solutions; (b) luminescent emission spectra of Cd-MOF dispersed in aqueous solution upon incremental addition of TNP.

https://doi.org/10.1021/acsomega.3c03073
ACS Omega 2023, 8, 24635−24643

that Cd-MOF can be used as a sensor for detecting FLU in aqueous media. To investigate the effect of FLU concentration on the fluorescence intensity of Cd-MOF, a quantitative experiment was conducted. The fluorescence intensity of Cd-MOF gradually decreased as the concentration of FLU increased from 0 to 12 μL (Figure 4b). At the FLU concentration of 12 μL, the fluorescence intensity of the complex reached the minimum, exhibiting linearity at low concentrations (5×10^{-6} to 3×10^{-5} M) (Figure S5). To further evaluate the effect of luminescent titration, the S−V equation was employed to calculate the quenching efficiency, with K_{SV} determined at a concentration of 120 μM. The calculated K_{SV} and LOD values are 2.269×10^{-5} M and 0.078 μmol/L.

Finally, an interference experiment was conducted (Figure S6). We added equal amounts of FLU solution to the Cd-MOF suspension containing other pesticides and studied the interference of other pesticides on the Cd-MOF system.[28] It was observed that the fluorescence intensity did not considerably decrease with the addition of other pesticides, but the fluorescence was almost completely quenched after the addition of equimolar amounts of FLU.[29−33] This suggests that the presence of other pesticides does not affect the quenching effect of FLU on the Cd-MOF system, indicating that Cd-MOF can selectively detect FLU with high sensitivity even in the presence of other pesticides.

3.3.3. Fluorescence Detection of Cd-MOF for Different NACs. Solutions (10 mmol/L) of the following nine NACs were prepared for fluorescence sensing tests: *p*-nitrophenol (4-NP), 2,4-dinitrophenylhydrazine (DNP), nitrobenzene (NB), 3-nitroaniline (3-NT), *p*-nitrobenzoic acid (PNBA), 2,4,6-tritrophenylhydrazine (TRI), *p*-nitrophenylhydrazine (4-NPH), *o*-nitroaniline (*O*-NT), and TNP. First, 3 mg of ground Cd-MOF was dispersed in 10 mL of distilled water, sonicated for 30 min, and left to stand at room temperature for 3 days before taking the supernatant for fluorescence experiments. Second, qualitative experiments were conducted on Cd-MOF, which was dispersed in different NAC solutions. The fluorescence of Cd-MOF was remarkably quenched after the addition of TNP (Figure 5a). The fluorescence intensity after the addition of other NACs does not substantially vary. Therefore, TNP caused the most pronounced quenching effect, demonstrating that Cd-MOF can be used as a sensor for detecting TNP in aqueous media. To investigate the effect of TNP concentration on the fluorescence intensity of Cd-MOF, a quantitative experiment was conducted. The fluorescence intensity of Cd-MOF gradually decreased as the concentration of TNP increased from 0 to 10 μL (Figure 5b). At the TNP concentration of 10 μL, the fluorescence intensity is at its lowest point, exhibiting linearity at low concentrations (1×10^{-5} to 5×10^{-5} M) (Figure S7). To further evaluate the effect of luminescent titration, the S−V equation was employed to calculate the quenching efficiency, with K_{SV} determined at a concentration of 100 μM. The calculated K_{SV} and LOD values were 1.470×10^{-5} M and 0.12 μmol/L. Finally, an interference experiment was conducted (Figure S8). The fluorescence intensity did not experience a remarkable decrease with the addition of other NACs but was almost completely quenched after the addition of equimolar amounts of TNP, indicating that the addition of TNP is not affected by the presence of other NACs. These results demonstrate that Cd-MOF is a promising fluorescence sensor for TNP with high sensitivity and selectivity.

3.4. Applications: Drug Testing. SECTs are effective drugs for the treatment of ulcerative colitis. However, their excessive use can cause severe side effects, such as red blood cell abnormalities, dizziness, and tinnitus. Thus, the dosage of sulfasalazine must be accurately controlled, necessitating a precise and reliable detection method. Sulfasalazine is chemically denoted as 5-[*p*-(2-pyridylsulfonyl) benzene] azosalicylic acid[34−38] and its structural formula is presented in Figure 6. For the experiment, SECTs were ground into a

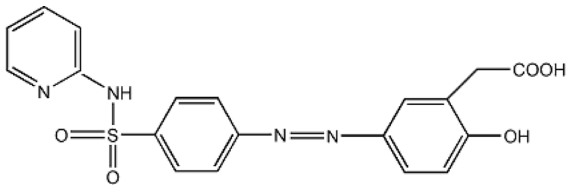

Figure 6. Chemical formulas for the main components of the drug.

powder and used to prepare an aqueous solution with a concentration of 1 mmol/L. Cd-MOF powder (3 mg) was then weighed and dispersed in 10 mL of distilled water. After ultrasonication for 30 min, it was allowed to stand for 3 days to form a stable suspension. We conducted qualitative experiments on the drug and found that Cd-MOF exhibited a remarkable quenching effect after the addition of SECTs (Figure 7a). To explore the specific relationship between the concentration of SECT and the fluorescence intensity of Cd-MOF, we conducted a quantitative experiment. The fluorescence intensity of Cd-MOF gradually decreased with the increase in SECT solution dosage from 0 to 120 μL (Figure 7b). At the SECT dosage of 120 μL, the fluorescence intensity of the complex reached the minimum, exhibiting linearity at low concentrations (2×10^{-6} to 1×10^{-5} M) (Figure S9). To further evaluate the effect of luminescent titration, the S−V equation ($I_0/I = 1 + K_{SV}[M]$) was employed to calculate the quenching efficiency, where I_0 is the initial luminescent intensity, I is the luminescent intensity after the addition of SECT, $[M]$ is the concentration of SECT, and K_{SV} is the quenching constant when the concentration is increased to 120 μM. The calculated K_{SV} and LOD values are 6.651×10^{-4} M and 0.26 μmol/L.

To alleviate the pain of medicated patients and facilitate swallowing, certain excipients, such as sucrose, glucose, starch, and lactose, are added to commercial SECTs. Therefore, the drug properties may be affected by these added excipients. In addition, large amounts of K^+, Na^+, Mg^{2+}, Fe^{3+}, and Ca^{2+} are present in the human body, which may also affect drug properties. To confirm whether these factors affect the obtained results, we conducted anti-interference experiments,[39−42] which demonstrated no remarkable decreases in fluorescent intensity with the addition of sucrose, glucose, starch, lactose, K^+, Na^+, Mg^{2+}, Fe^{3+}, and Ca^{2+} ion solutions. At the same time, luminescence is almost completely quenched after the addition of equimolar amounts of sulfasalazine, indicating that the detection of sulfasalazine is not affected by the presence of these ions and compounds (Figure S10). Thus, anti-interference experiments showed that Cd-MOF demonstrates excellent selectivity for sulfasalazine.

3.5. Fluorescence Quenching Mechanism. Elucidating the mechanism of fluorescence quenching is crucial for understanding the properties of fluorescence analyses and probes. Therefore, we investigated the mechanism of

https://doi.org/10.1021/acsomega.3c03073
ACS Omega 2023, 8, 24635−24643

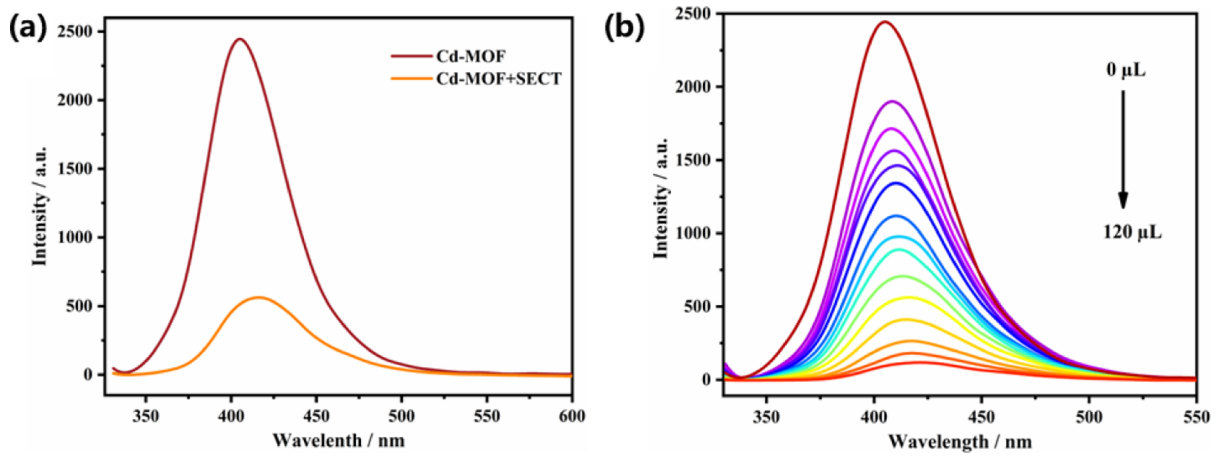

Figure 7. (a) Fluorescence spectra of Cd-MOF dispersed in SECT solutions; (b) luminescent emission spectra of Cd-MOF dispersed in aqueous solution upon incremental addition of SECT.

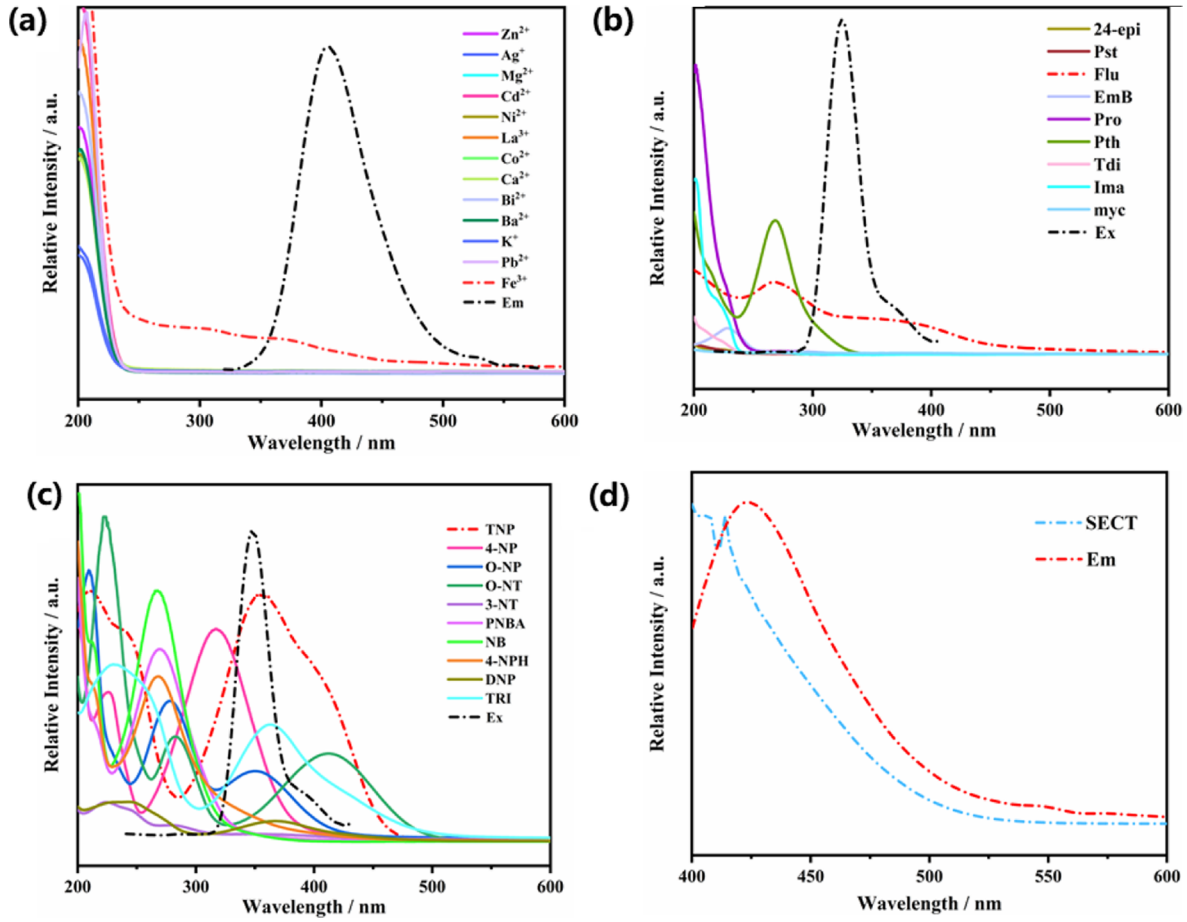

Figure 8. (a) UV absorption spectrum of cations and emission spectrum of Cd-MOF; (b) UV absorption spectrum and Cd-MOF excitation spectrum of pesticides; (c) UV absorption and excitation spectra of nitro explosive Cd-MOF; (d) UV absorption spectrum of SECT and emission spectrum of Cd-MOF.

fluorescence quenching of Cd-MOF caused by the above analytes. The mechanism of luminescence quenching can generally be explained by the following points: (1) the collapse of the MOF skeleton; (2) resonance energy transfer and competitive absorption; (3) solidification effect: the organic ligands in MOF can solidify during adsorption, which restricts the free movement of fluorescent molecules and weakens the fluorescence signal; (4) solvent effect: the solvent molecules surrounding the fluorescent molecules in MOF can affect the fluorescence signal intensity.[43−46] In some cases, solvent molecules can cause static quenching of fluorescent molecules, leading to the weakening of the fluorescence signal. Several experiments were conducted to determine the possible fluorescence mechanism.[47−52] The PXRD spectra of the sample and the simulated PXRD spectra remain nearly unchanged after the fluorescence test (Figure S1), indicating

https://doi.org/10.1021/acsomega.3c03073
ACS Omega 2023, 8, 24635−24643

that skeleton collapse is not the cause of fluorescence quenching.

Another method is to compare the overlapping regions of the UV−vis absorption spectrum of the analyte with the excitation or emission spectrum of Cd-MOF.[53] This method can explain whether the fluorescence quenching of Cd-MOF is caused by resonance energy transfer or competitive absorption.[54−56] When the absorption spectrum of the UV−vis analyte and the emission spectrum of Cd-MOF overlap, luminescence quenching of Cd-MOF may occur; this is known as resonance energy transfer quenching. In contrast, when the UV−vis absorption spectrum of the responder and the excitation spectrum of Cd-MOF overlap, competitive absorption may cause Cd-MOF fluorescence quenching via the analyte. In the study of cations, we found that the UV−vis absorption spectrum of Fe^{3+} almost completely overlaps with the emission spectrum of Cd-MOF (Figure 8a), suggesting that the quenching mechanism is resonance energy transfer. In the study of pesticides and nitro explosives, the UV−vis absorption spectra of FLU and TNP almost completely overlap with the excitation spectra of Cd-MOF, suggesting that the quenching mechanism of Cd-MOF is competitive absorption for both FLU and TNP (Figure 8b,c).

According to the above quenching mechanism, the UV−vis absorption spectrum of sulfasalazine almost completely overlaps with the emission spectrum of Cd-MOF, indicating that the fluorescence quenching mechanism of sulfasalazine is resonance energy transfer (Figure 8d).

4. CONCLUSIONS

In this paper, a Cd-MOF with a 2D network structure constructed from Cd^{2+} crosslinked by $(ttc)^{2-}$ ligands was synthesized via a solvothermal method. The prepared Cd-MOF showed excellent fluorescence performance and is a highly sensitive and selective luminescence sensor for Fe^{3+}, FLU, TNP, and sulfasalazine. The excellent quenching behaviors of Fe^{3+} (LOD = 5.34×10^{-8} M) and SECT (LOD = 2.67×10^{-7} M) were attributed to energy transfer. The remarkable quenching behavior of FLU (LOD = 7.8×10^{-8} M) and TNP (LOD = 1.21×10^{-7} M) is attributed to the results of resonance competitive absorption. Notably, the highly sensitive detection of sulfasalazine was realized in aqueous solutions, which is expected to play an important role in medical detection.

■ ASSOCIATED CONTENT

Supporting Information

The Supporting Information is available free of charge at https://pubs.acs.org/doi/10.1021/acsomega.3c03073.

PXRD diagram of Cd-MOF; TGA pattern of Cd-MOF; linear diagram and anti-interference diagram of Fe^{3+}, FLU, TNP, and SECT; crystal data and structure refinement for Cd-MOF; selected bond distances/nm and bond angles/° for Cd-MOF; and hydrogen bond distances (nm) and bond angles (°) for Cd-MOF (PDF)

■ AUTHOR INFORMATION

Corresponding Author

Hua-li Cui − *Shaanxi Key Laboratory of Chemical Reaction Engineering, College of Chemistry and Chemical Engineering, Yan'an University, Yan'an 716000, P. R. China;* Email: cuihuali07@163.com

Authors

Wen Liu − *Shaanxi Key Laboratory of Chemical Reaction Engineering, College of Chemistry and Chemical Engineering, Yan'an University, Yan'an 716000, P. R. China;* orcid.org/0000-0002-4161-0214

Jie Zhou − *Shaanxi Key Laboratory of Chemical Reaction Engineering, College of Chemistry and Chemical Engineering, Yan'an University, Yan'an 716000, P. R. China*

Zi-tong Su − *Shaanxi Key Laboratory of Chemical Reaction Engineering, College of Chemistry and Chemical Engineering, Yan'an University, Yan'an 716000, P. R. China*

You-zhen Zhang − *Shaanxi Key Laboratory of Chemical Reaction Engineering, College of Chemistry and Chemical Engineering, Yan'an University, Yan'an 716000, P. R. China*

Xiao-li Chen − *Shaanxi Key Laboratory of Chemical Reaction Engineering, College of Chemistry and Chemical Engineering, Yan'an University, Yan'an 716000, P. R. China*

Er-lin Yue − *Shaanxi Key Laboratory of Chemical Reaction Engineering, College of Chemistry and Chemical Engineering, Yan'an University, Yan'an 716000, P. R. China;* orcid.org/0000-0002-1161-1953

Complete contact information is available at: https://pubs.acs.org/10.1021/acsomega.3c03073

Notes

The authors declare no competing financial interest.

■ ACKNOWLEDGMENTS

This work was supported by the National Natural Science Foundation of China (no. 21763028), the Science and Technology Project of Shaanxi Province (nos. 2022QFY07-05 and 2022NY-071), and the Science and Technology Project of Yan'an Province (no. 2022SLJBZ-002).

■ REFERENCES

(1) Zhao, S.; Xiao, J.; Zheng, T.; Liu, M.; Wu, H.; Liu, Z. Highly Selective and Sensitive Detection of PO_4^{3-} Ions in Aqueous Solution by a Luminescent Terbium Metal-Organic Framework. *ACS Omega* **2019**, *4*, 16378−16384.

(2) Yang, Z.-R.; Wang, M.-M.; Wang, X.-S.; Yin, X.-B. Boric-Acid-Functional Lanthanide Metal-Organic Frameworks for Selective Ratiometric Fluorescence Detection of Fluoride Ions. *Anal. Chem.* **2017**, *89*, 1930−1936.

(3) Wang, Z.-J.; Qin, L.; Chen, J.-X.; Zheng, H.-G. H-Bonding Interactions Induced Two Isostructural Cd(II) Metal−Organic Frameworks Showing Different Selective Detection of Nitroaromatic Explosives. *Inorg. Chem.* **2016**, *55*, 10999−11005.

(4) Thangavelu, D.; Chen, Y.; Annamalai, P.; Ramadoss, M.; Narayanan, V. Rationally Designed Ag@polymer@2-D LDH Nanoflakes for Bifunctional Efficient Electrochemical Sensing of 4-Nitrophenol and Water Oxidation Reaction. *ACS Appl. Mater. Interfaces* **2022**, *14*, 6518−6527.

(5) Xu, W.; Chen, H.; Xia, Z.; Ren, C.; Han, J.; Sun, W.; Wei, Q.; Xie, G.; Chen, S. A Robust Tb(III)-MOF for Ultrasensitive Detection of Trinitrophenol: Matched Channel Dimensions and Strong Host-Guest Interactions. *Inorg. Chem.* **2019**, *58*, 8198−8207.

(6) Chai, H.-M.; Zhang, G.-Q.; Jiao, C.-X.; Ren, Y.-X.; Gao, L.-J. A Multifunctional Tb-MOF Detector for H_2O_2, Fe^{3+}, $Cr_2O_7^{2-}$, and TPA Explosive Featuring Coexistence of Binuclear and Tetranuclear Clusters. *ACS Omega* **2020**, *5*, 33039−33046.

(7) Seal, N.; Palakkal, A.-S.; Singh, M.; Goswami, R.; Pillai, R.-S.; Neogi, S. Chemically Robust and Bifunctional Co(II)-Framework for Trace Detection of Assorted Organo-toxins and Highly Cooperative Deacetalization−Knoevenagel Condensation with Pore-Fitting-In-

duced Size-Selectivity. *ACS Appl. Mater. Interfaces* **2021**, *13*, 28378−28389.
(8) Yu, H.; Fan, M.; Liu, Q.; Su, Z.; Li, X.; Pan, Q.; Hu, X. Two Highly Water-Stable Imidazole-Based Ln-MOFs for Sensing Fe^{3+},$Cr_2O_7^{2-}$/CrO_4^{2-} in a Water Environment. *Inorg. Chem.* **2020**, *59*, 2005−2010.
(9) Farinas, P.-S.; Doimo, A.-L.; da Silva, M. A. R.; Teixeira, I.-F. Synthesis and Application of Ag Nanoparticles for an Undergraduate Laboratory: Ultrasensitive Method to Detect Copper(II) Ions. *J. Chem. Educ.* **2020**, *97*, 3771−3777.
(10) Wang, W.; Yang, J.; Wang, R.; Zhang, L.; Yu, J.; Sun, D. Luminescent Terbium-Organic Framework Exhibiting Selective Sensing of Nitroaromatic Compounds (NACs). *Cryst. Growth Des.* **2015**, *15*, 2589−2592.
(11) Gu, Y.-N.; Lu, J.-F.; Liu, H.; Zhao, B.; Zhou, X.-H.; Zhao, Y.-Q.; Sun, Q.-Z.; Zhang, B.-G. Two Eu^{3+} Based Complexes Containing Uncoordinated Lewis Basic Pyridyl Sites and Chemical Sensing of 4-Nitrophenol and Fe^{3+} ions. *Cryst. Growth Des.* **2022**, *22*, 4874−4884.
(12) Wang, H.-M.; Feng, X.-N.; Xia, Y.; Yin, X.-B. Dual-Ligand Terbium Metal−Organic Framework for Visual Ratiometric Fluorescence Sensing of Nitrites in Pickles. *ACS Food Sci. Technol.* **2022**, *2*, 1911−1920.
(13) You, Z.-X.; Xiao, Y.; Guan, Q.-L.; Xing, Y.-H.; Bai, F.-Y.; Xu, F. Cage Bismuth Metal-Organic Framework Materials Based on a Flexible Triazine-Polycarboxylic Acid: Subgram Synthesis, Application for Sensing, and White Light Tuning. *Inorg. Chem.* **2022**, *61*, 13893−13914.
(14) Bai, C.; Yan, L.; Hu, H.-M.; Zou, F.; Zhang, T.-H.; Xue, G. Electrospinning Fabrication of Europium-Chain@polymer Nanofiber Films for Visual Detection of the Fe^{3+} Ion. *ACS Appl. Polym. Mater.* **2021**, *3*, 4504−4511.
(15) Sheldrick, G.-M. Crystal Structure Refinement with SHELXL. *Acta Crystallogr., Sect. C: Struct. Chem.* **2015**, *71*, 3−8.
(16) Alhaddad, M.; Sheta, S.-M. Dual Naked-Eye and Optical Chemosensor for Morphine Detection in Biological Real Samples Based on Cr(III) Metal-Organic Framework Nanoparticles. *ACS Omega* **2020**, *5*, 28296−28304.
(17) Ferguson, T.; Bernicky, A.; Kozin, I.; Loock, H.-P. HPLC-Detector Based on Hadamard-Transform Fluorescence Excitation-Emission-Matrix Spectroscopy. *Anal. Chem.* **2021**, *93*, 8116−8121.
(18) Mohamed, S.-H.; Salim, A.-I.; Issa, Y.-M.; Ali, A.-E. Detection and Identification of Adulteration in Vinegar Samples Based on Reversed-Phase High-Performance Liquid Chromatographic (RP-HPLC) Strategies. *ACS Food Sci. Technol.* **2022**, *2*, 21−30.
(19) Kumar, S.; Ma, S.; Mohan, B.; Li, S.; Ren, P. Triazole-Based Cu(I) Cationic Metal-Organic Frameworks with Lewis Basic Pyridine Sites for Selective Detection of Ce^{3+} Ions. *Inorg. Chem.* **2022**, *61*, 14778−14786.
(20) Wang, Y.; Gao, W.; Li, Y.; Xiao, Y.; Song, W.; Yao, T.; Cheng, M.; Wang, W.; Hou, R. Establishment of a HPLC−MS/MS Detection Method for Glyphosate, Glufosinate-Ammonium, and Aminomethyl Phosphoric Acid in Tea and Its Use for Risk Exposure Assessment. *J. Agric. Food Chem.* **2021**, *69*, 7969−7978.
(21) Zhang, G.-L.; Zhang, M.; Shi, Q.; Jiang, Z.; Tong, L.; Chen, Z.; Tang, B. In Situ Construction of COF-Based Paper Serving as a Plasmonic Substrate for Enhanced PSI-MS Detection of Polycyclic Aromatic Hydrocarbons. *ACS Appl. Mater. Interfaces* **2021**, *13*, 43438−43448.
(22) Wang, X.-N.; Li, B. Monolithic Gold Nanoparticles/Thiol-*β*-cyclodextrin-Functionalized TiO2 Nanowires for Enhanced SALDI MS Detection and Imaging of Natural Products. *Anal. Chem.* **2022**, *94*, 952−959.
(23) Wu, J.; Huang, S.; Tan, L.; Li, Y.; Wu, X.; Liang, Y. Detection of Dengue Fever Nonstructural Protein 1 Antigen by Proteolytic Peptide Imprinting Technology and UHPLC−MS/MS. *Anal. Chem.* **2021**, *93*, 14106−14112.
(24) Liu, S.; Tao, D.; Liao, Y.; Yang, Y.; Sun, S.; Zhao, Y.; Yang, P.; Tang, Y.; Chen, B.; Liu, Y.; Xie, S.; Tang, Z. Highly Sensitive CRISPR/Cas12a-Based Fluorescence Detection of Porcine Reproductive and Respiratory Syndrome Virus. *ACS Synth. Biol.* **2021**, *10*, 2499−2507.
(25) Wu, F.-N.; Zhu, J.; Weng, G.-J.; Li, J.-J.; Zhao, J.-W. Tyrosine-Decorated Gold Nanoclusters Chelated Cerium(III) for Fluorescence Detection of Dopamine. *ACS Appl. Nano Mater.* **2021**, *4*, 13501−13509.
(26) Lei, M.; Jia, Y.; Zhang, W.; Xie, J.; Xu, Z.; Wang, Y.; Du, W.; Liu, W. Ultrasensitive and Selective Detection of Uranium by a Luminescent Terbium−Organic Framework. *ACS Appl. Mater. Interfaces* **2021**, *13*, 51086−51094.
(27) Praveen, L.; Reddy, M.-L.-P.; Varma, R.-L. Dansyl-Styrylquinoline Conjugate as Divalent Iron Sensor. *Tetrahedron Lett.* **2010**, *51*, 6626−6629.
(28) Moon, S.-Y.; Cha, N.-R.; Kim, Y.-H.; Chang, S.-K. New Hg^{2+}-Selective Chromo- and Fluoroionophore Based upon 8-Hydroxyquinoline. *J. Org. Chem.* **2004**, *69*, 181−183.
(29) Zhang, H.; Wang, Q.-L.; Jiang, Y.-B. 8-Methoxyquinoline Based Turn-on Metal Fluoroionophores. *Tetrahedron Lett.* **2007**, *48*, 3959−3962.
(30) Prodi, L.; Bargossi, C.; Montalti, M.; Zaccheroni, N.; Su, N.; Bradshaw, J.-S.; Izatt, R.-M.; Savage, P.-B. An Effective Fluorescent Chemosensor for Mercury Ions. *J. Am. Chem. Soc.* **2000**, *122*, 6769−6770.
(31) Liu, X.; Theil, E.-C. Ferritins: Dynamic Management of Biological Iron and Oxygen Chemistry. *Acc. Chem. Res.* **2005**, *38*, 167−175.
(32) Gray, H.-B.; Winkler, J.-R. Electron Transfer in Proteins. *Annu. Rev. Biochem.* **1996**, *65*, 537−561.
(33) Zhou, Y.; Chen, H.-H.; Yan, B. An Eu^{3+} Post-Functionalized Nanosized Metal−Organic Framework for CationExchange-Base-dFe^{3+}-Sensing in an Aqueous Environment. *J. Mater. Chem. A* **2014**, *2*, 13691−13697.
(34) Yang, C.-X.; Ren, H.-B.; Yan, X.-P. Fluorescent Metal−Organic Framework MIL-53(Al) for Highly Selective and Sensitive Detection of Fe^{3+} in Aqueous Solution. *Anal. Chem.* **2013**, *85*, 7441−7446.
(35) Chen, Z.; Sun, Y.-W.; Zhang, L.-L.; Sun, D.; Liu, F.; Meng, Q.-G.; Wang, R.-M.; Sun, D.-F. A Tubular Europium-Organic Framework Exhibiting Selective Sensing of Fe^{3+} and Al^{3+} over Mixed Metal Ions. *Chem. Commun.* **2013**, *49*, 11557−11559.
(36) Zheng, M.; Tan, H.-Q.; Xie, Z.-G.; Zhang, L.-G.; Jing, X.-B.; Sun, Z.-C. Fast Response and High Sensitivity Europium Metal Organic Framework Fluorescent Probe with Chelating Terpyridine Sites for Fe^{3+}. *ACS Appl. Mater. Interfaces* **2013**, *5*, 1078−1083.
(37) Lu, Y.; Yan, B.; Liu, J.-L. Nanoscale Metal−Organic Frameworks as Highly Sensitive Luminescent Sensors for Fe^{2+} in Aqueous Solution and Living Cells. *Chem. Commun.* **2014**, *50*, 9969−9972.
(38) Chen, J.-L.; Zhuo, S.-J.; Wu, Y.-Q.; Fang, F.; Li, L.; Zhu, C.-Q. High Selective Determination Iron(II) by Its Enhancement Effect on the Fluorescence of Pyrene-Tetramethylpiperidinyl (TEMPO) as a Spin Fluorescence Probe. *Spectrochim. Acta, Part A* **2006**, *63*, 438−443.
(39) Li, P.; Fang, L.-B.; Zhou, H.; Zhang, W.; Wang, X.; Li, N.; Zhong, H.; Tang, B. A New Ratiometric Fluorescent Probe for Detection of Fe^{2+} with High Sensitivity and Its Intracellular Imaging Applications. *Chem.—Eur. J.* **2011**, *17*, 10520−10523.
(40) Li, L.-J.; Tang, S.-F.; Wang, C.; Lv, X.-X.; Jiang, M.; Wu, H.-Z.; Zhao, X.-B. High Gas Storage Capacities and Stepwise Adsorption in a UiO Type Metal−Organic Framework incorporating Lewis Basic Bipyridyl Sites. *Chem. Commun.* **2014**, *50*, 2304−2307.
(41) Gándara, F.; Furukawa, H.; Lee, S.; Yaghi, O.-M. High Methane Storage Capacity in Aluminum Metal−Organic Frameworks. *J. Am. Chem. Soc.* **2014**, *136*, 5271−5274.
(42) Maity, D.; Govindaraju, T. Pyrrolidine Constrained Bipyridyl-dansyl Click Fluoroionophore as Selective Al^{3+} Sensor. *Chem. Commun.* **2010**, *46*, 4499−4501.
(43) Cui, Y.; Zhu, F.; Chen, B.; Qian, G. Metal−Organic Frameworks for Luminescence Thermometry. *Chem. Commun.* **2015**, *51*, 7420−7431.

https://doi.org/10.1021/acsomega.3c03073
ACS Omega 2023, 8, 24635−24643

(44) Gupta, A.; Kumar, N. A Review of Mechanisms for Fluorescent "Turn-On" Probes to Detect Al^{3+} Ions. *RSC Adv.* **2016**, *6*, 106413−106434.
(45) Das, S.; Dutta, M.; Das, D. Fluorescent Probes for Selective Determination of Trace Level Al^{3+}: Recent Developments and Future Prospects. *Anal. Methods* **2013**, *5*, 6262−6285.
(46) Valeur, B.; Leray, I. Design Principles of Fluorescent Molecular Sensors for Cation Recognition. *Coord. Chem. Rev.* **2000**, *205*, 3−40.
(47) Hazra, A.; Roy, A.; Mukherjee, A.; Maiti, G.-P.; Roy, P. Remarkable Difference in Al^{3+} and Zn^{2+} Sensing Properties of Quinoline Based Isomers. *Dalton Trans.* **2018**, *47*, 13972−13989.
(48) Jiang, X.-H.; Wang, B.-D.; Yang, Z.-Y.; Liu, Y.-C.; Li, T.-R.; Liu, Z.-C. 8-Hydroxyquinoline-5-carbaldehyde Schiff-base as a Highly Selective and Sensitive Al^{3+} Sensor in Weak Acid Aqueous Medium. *Inorg. Chem. Commun.* **2011**, *14*, 1224−1227.
(49) Qin, J.-C.; Yang, Z.-Y.; Fan, L.; Cheng, X.-Y.; Li, T.-R.; Wang, B.-D. Design and Synthesis of a Chemosensor for the Detection of Al^{3+} Based on ESIPT. *Anal. Methods* **2014**, *6*, 7343−7348.
(50) Das, M.-C.; Xiang, S.; Zhang, Z.; Chen, B. Functional Mixed Metal-Organic Frameworks with Metalloligands. *Angew. Chem., Int. Ed.* **2011**, *50*, 10510−10520.
(51) Zhao, X.; Shimazu, M.-S.; Chen, X.; Bu, X.; Feng, P. Homo-Helical Rod Packing as a Path Toward the Highest Density of Guest-Binding Metal Sites in Metal-Organic Frameworks. *Angew. Chem., Int. Ed.* **2018**, *57*, 6208−6211.
(52) Gao, J.; Miao, J.; Li, P.-Z.; Teng, W.-Y.; Yang, L.; Zhao, Y.; Liu, B.; Zhang, Q. A p-Type Ti(IV)-Based Metal-Organic Framework with Visible-Light Photo-Response. *Chem. Commun.* **2014**, *50*, 3786−3788.
(53) Hu, Y.; Ding, M.; Liu, X.-Q.; Sun, L.-B.; Jiang, H.-L. Rational Synthesis of an Exceptionally Stable Zn(II) Metal-Organic Framework for the Highly Selective and Sensitive Detection of Picric Acid. *Chem. Commun.* **2016**, *52*, 5734−5737.
(54) Wu, J.; Liu, W.; Ge, J.; Zhang, H.; Wang, P. New Sensing Mechanisms for Design of Fluorescent Chemosensors Emerging in Recent Years. *Chem. Soc. Rev.* **2011**, *40*, 3483−3495.
(55) Padalkar, V.-S.; Seki, S. Excited-State Intramolecular Proton-Transfer (ESIPT)-Inspired Solid State Emitters. *Chem. Soc. Rev.* **2016**, *45*, 169−202.
(56) Meng, F.-Y.; Chen, Y.-A.; Chen, C.-L.; Chou, P.-T. Syntheses and Excited-State Intramolecular Proton Transfer of 3-Hydroxythioflavone and Its Sulfone Analogue. *ChemPhotoChem* **2018**, *2*, 475−480.

https://doi.org/10.1021/acsomega.3c03073
ACS Omega 2023, 8, 24635−24643